Supplementary Material

OH and HO_2 Radical Chemistry during PROPHET 2008 and CABINEX 2009 – Part 1: Measurements and Model Comparison

S. M. Griffith[1,2], R. F. Hansen[2,3], S. Dusanter[1,4,5], P. S. Stevens[1,2,3], M. Alaghmand[6], S. B. Bertman[7], M. A. Carroll[8,9], M. Erickson[10], M. Galloway[11†], N. Grossberg[12], J. Hottle[11], J. Hou[13], B. T. Jobson[10], A. Kammrath[11], F. N. Keutsch[11], B. L. Lefer[12], L. H. Mielke[6,*], A. O'Brien[14‡], P. B. Shepson[6,15], M. Thurlow[14], W. Wallace[10], N. Zhang[13], X. L. Zhou[13]

[1]School of Public and Environmental Affairs, Indiana University, Bloomington, IN USA
[2]Center for Research in Environmental Science, Indiana University, Bloomington, IN USA
[3]Department of Chemistry, Indiana University, Bloomington, IN USA
[4]Université Lille Nord de France, Lille, France
[5]École des Mines de Douai, Douai, France
[6]Department of Chemistry, Purdue University, West Lafayette, IN
[7]Department of Chemistry, Western Michigan University, Kalamazoo, MI
[8]Department of Chemistry, University of Michigan, Ann Arbor, MI
[9]Department of Atmospheric, Oceanic, and Space Sciences, University of Michigan, Ann Arbor, MI
[10]Department of Civil and Environmental Engineering, Washington State University, Pullman, WA
[11]Department of Chemistry, University of Wisconsin-Madison, Madison, WI
[12]Department of Earth and Atmospheric Sciences, University of Houston, Houston, TX
[13]School of Public Health, State University of New York at Albany, Albany, NY
[14]Department of Chemistry and Chemical Biology, Harvard University, Cambridge, MA
[15]Department of Earth and Atmospheric Sciences, Purdue University, West Lafayette, IN

[†]Now at: Departmet of Chemistry and Biochemistry, University of San Diego, San Diego, CA
[*]Now at: School of Public and Environmental Affairs, Indiana University, Bloomington, IN
[‡]Now at: Civil and Environmental Engineering, Princeton University, Princeton, NJ

Correspondence to: S.M. Griffith (stegriff@indiana.edu)

Details of PROPHET 2008 and CABINEX 2009

At the PROPHET site, a Pyrex sampling manifold runs from the top of the 32 meter tower to the laboratory where several instruments sampled ambient air during both years. Notable exceptions in absence of sampling from the manifold besides the OH and HO_2 measurements were that during CABINEX 2009 Washington State University had set up their own sampling lines for NO_x and VOC measurements that allowed them to switch between multiple heights from the ground (6 m), within-canopy (20 m), and above-canopy (31 m).

Sec. S1: IU-FAGE calibration

While IU-FAGE is extensively calibrated before and after field campaigns, routine field calibrations are also necessary to track the instrumental sensitivity that may drift due to changing operating conditions (chamber pressure, spectral laser band-width, beam alignment (Creasey et al., 2001)). Calibration of IU-FAGE was performed using the water-vapor UV-photolysis technique that relies on the photolysis of water at 184.9 nm and reactions R3 and R4 to produce OH and HO_2 radicals (Tanner and Eisele, 1995; Creasey et al., 1997; Holland et al., 1998; Matsumi et al., 2002; Faloona et al., 2004; Smith et al., 2006; Dusanter et al., 2008). A set of bubblers and a calibration tool fitted with a 184.9 nm Hg lamp was used to humidify air, photolyze the water vapor, and overflow the IU-FAGE inlet with a calibrated flow of HO_x radicals (Dusanter et al., 2008). The concentrations of OH and HO_2 radicals produced in reactions R1 and R2 can be calculated using Eq. 1:

$$H_2O + h\nu(184.9nm) \rightarrow OH + H \qquad \text{(R1)}$$

$$H + O_2 + M \rightarrow HO_2 + M \qquad \text{(R1)}$$

$$[OH]=[HO_2]=[H_2O]\times\sigma_{water}\times\phi_{OH+H}\times(F\times t) \quad \text{(Eq.1)}$$

Here σ_{water} and ϕ_{OH+H} are the absorption cross-section of water (Cantrell et.al. 1997; Hofzumahaus et.al. 1997; Creasey et al., 2000) and the photodissociation quantum yield of reaction R3 (Sander et al., 2011). The water vapor mixing ratio inside the calibration system is measured with a Li-6262 CO_2/H_2O Gas Analyzer (LICOR). The product of the photon flux (F) and photolysis time (t) is calculated using O_2 actinometry based on the photolysis of oxygen at 184.9 nm that produces ozone (Eqs. 2 and 3), where the quantum yield of the oxygen photolysis is equal to 2 due to each $O(^3P)$ molecule leading to an ozone molecule via reaction with another oxygen (R5 and R6):

$$O_2+h\nu\rightarrow O(^3P)+O(^3P) \quad \text{(R3)}$$

$$O(^3P)+O_2(+M)\rightarrow O_3 \quad \text{(R4)}$$

$$[O_3]=[O_2]\times\sigma_{O_2}\times\phi_{O_3}\times(F\times t) \quad \text{(Eq. 2)}$$

$$(F\times t)=\frac{[O_3]}{2[O_2]\sigma_{O_2}} \quad \text{(Eq. 3)}$$

The mixing ratio of O_3 produced during photolysis was originally measured during every calibration with a Teledyne 400E Ozone monitor. However, tracking ozone during each calibration became unreasonable due to the time required to perform a precise measurement of the low ozone mixing ratio produced in the calibrator. To improve the time response for each calibration, a photodiode was installed on the calibration tube to track the photon flux from the Hg-lamp. This fast photometric reading was then used as a calibrated proxy to calculate the mixing ratio of O_3.

The amount of O_3 produced in the calibrator is periodically checked during laboratory characterizations of IU-FAGE. Thus the quantity (F × t) derived from the ozone mixing ratio is then used to calculate the concentration of OH produced by the calibration system through Eq. 1 (Current Laboratory Specs: 17% calibration accuracy; Limit of Detection (LOD) = 3×10^5 cm^{-3},15min average for OH and 1.0×10^7 cm^{-3} for 30 sec. average for HO_2*).

Between the PROPHET 2008 and CABINEX 2009 campaigns, the IU-FAGE inlet was modified to improve the sensitivity and LOD. It was found at the PROPHET site that changing the pinhole from a 0.025" to 0.040" diameter used previously improved the instrument sensitivity by 30% for a given laser power. The larger pinhole increasing the linear flow velocity, potentially reducing OH loss on the inlet, and the increase in pressure leading to a greater density of sampled air could have both contributed to the greater sensitivity. In addition, following the CABINEX 2009 campaign a temperature-controlled housing with a drying agent was constructed to minimize condensation forming on the entrance window of the multipass cell and to prevent small shifts in the alignment of the mounting bracket supporting the optical fiber.

Sec. S2 - Ozone × Water × Power Interference

Calibrations in the laboratory have quantified the response of IU-FAGE to the reaction sequence of R5 and R6 by sending known mixing ratios of ozone and water in zero-air to the IU-FAGE cell. Ozone is generated through reactions R3 and R4 with a low-pressure mercury pen-lamp (UVP 90-0012-01 (11SC-1)) set in a cell where dry zero-air is passed to avoid photolysis of water vapor. The calibration air stream is then humidified, and then sampled for ozone, water, and eventually sampled by the IU-FAGE instrument. When normalized to 1 ppbv of O_3, 1% of water, and 1 mW of laser power this interference is equivalent to 8500 ± 800 (2σ) molecule cm^{-3}

of OH (Figure S1). Typical values of this interference during PROPHET 2008 and CABINEX 2009 were below 2.5 x 10^5 molecules cm^{-3}.

$$O_3 + h\nu \rightarrow O(^1D) + O_2 \qquad \text{(R5)}$$

$$O(^1D) + H_2O \rightarrow OH + OH \qquad \text{(R6)}$$

After CABINEX, a gas-injector system was installed to overflow the sampling inlet with perfluoropropylene (C_3F_6) to quantify interferences by removing ambient OH in the sampled air mass. The advantage of this new design over an internal addition of C_3F_6 to the low-pressure region (Faloona et al., 2001, Stevens et al., 1994) is that additional interferences due to the low pressure sampling can be determined in addition to any laser generated OH during ambient measurements. This is made possible by the lower C_3F_6 concentration inside the low-pressure region of the FAGE instrument minimizing the removal of OH molecules that may be produced from the decomposition of unstable compounds when the sampled air mass travels from the inlet to the detection region. The scrubbing efficiency of OH by this external C_3F_6 addition was found to reach 95% at a flow of 5 sccm.

Ground-based interference testing was performed at the PROPHET site during the summer of 2010 to quantify the total interference on the OH measurement using this C_3F_6 external scrub technique. The results showed that the total measured interference is consistent with the ozone-water interference described above (Figure S2), which suggests that the performance of IU-FAGE at the PROPHET site in 2008 and 2009 may be free of unknown interferences. To quantify a potential additional interference, the maximum difference in the uncertainty ranges can be examined between the calculated and measured interference values. When accounting for

the reach of the uncertainty bars, the maximum underprediction by the calculated interference is 5×10^5 molecules cm^{-3}, while most values are well below this level.

Sec. S3 - Modeling Details

As stated in the main text, Figure 3 shows the median model constraint values measured from above canopy at the PROPHET site during 2008 and CABINEX 2009. The days that these measurements span for the 2 years varies within the time frame of early July to mid August as follows (2008, 2009): temperature (0701-0808, 0701-0808), j-values (0706-0803, 0704-0808), NO_x (0701-0725, 0708-0808), ozone (0701-0808, 0701-0808), HONO (0711-0807, 0701-0806), Isoprene (0706-0808, 0721-0808), MACR + MVK (0706-0808, 0721-0808), HCHO (0726-0814, 0721-0808), monoterpenes (0719-0812, 0721-0808). Also as stated in the main text, Table S2 provides information about the data coverage between 2008 and 2009, and illustrates that there are fewer overlapping data points in 2008 for the median campaign modeling vs. measured HO_x comparison, where only periods when measurements of isoprene, NO, and OH overlapped were analyzed. As an example of the ability of the median campaign modeled values to represent the bulk of the campaign, Figure S3 shows the difference in comparing the median measured constraint values for the months of July 2008 and 2009, and shows that only using the overlapping times of analysis for the two campaigns does affect the data constraining the model and should be kept in mind in comparing these campaign median constraints.

Table S1 details how each constraint dataset was arrived at for use in the RACM/MIM mechanism in both years. These constraints were either measured (as noted in the main text and in Table 2) or estimated depending on their availability in 2008 and 2009 (Table S2). For measurements of NOx, conversion of NO to NO2 in the sampling line was not taken into account,

which could have contributed to approximately 9% conversion of NO to NO2 in 2008 and approximately 6% conversion in 2009. In 2008, HCHO measurements began a few days after the measurements of nitric oxide stopped which was the last day included in this analysis. A linear relationship between HCHO and O_3 was derived (R^2 = 0.56) from simultaneous measurements of these species from the subsequent weeks in 2008 and was used to estimate HCHO mixing ratios for this analysis. The correlation between ozone and HCHO appears to be different between 1998, 2008, and 2009 (Figure S4). While a positive relationship is observed for all 3 years, the slope is different between 2008 and 2009 and the relationship is not even linear in 1998. As a result, the estimated peak 2008 HCHO mixing ratios are approximately 2-2.5 times greater than at CABINEX. Formaldehyde was given an uncertainty of 100% for the 2008 Monte Carlo uncertainty analysis. However, a sensitivity analysis from the CABINEX modeling revealed that changing the HCHO mixing ratios by a factor of 2 had less than a 5% effect on OH and HO2+ISOP concentrations, suggesting that this difference in the 2008 estimated HCHO mixing ratios does not have a major impact on the modeling results for 2008.

Measurements of acetaldehyde, the main component of the aldehydes surrogate (ALD), were not performed during PROPHET 2008. CABINEX 2009 PTR-MS data suggests that acetaldehyde is roughly 1/3 of the HCHO mixing ratio (R^2 = 0.25). Overlapping times of acetaldehyde and HCHO in 1998 are sparse, but Tan et al. (2001) gives the median values of 2.7 ppbv and 3.8 ppbv for each suggesting that acetaldehyde is approximately 75% of the HCHO mixing ratio. Using these estimates from 2009 and 1998, 2008 acetaldehyde mixing ratios were estimated as 50% of HCHO mixing ratios. The model outputs are even less sensitive to the ALD mixing ratios than HCHO, and as a result the uncertainty associated with estimating these mixing ratios does not significantly impact the modeling results.

Monoterpene measurements in 2008 did not always overlap with the analysis periods compiled here. For periods where the monoterpene measurements did not coincide with the analysis, model surrogates API and LIM were constrained using the median monoterpene measurements using a breakdown of 90% API and 10% LIM based on observations during PROPHET 1998 (Table S3). The 90/10 monoterpene composition breakdown was also used during times where monoterpene measurements were available for the 2008 and 2009, as the measurements from the PTR-LIT in 2008 and PTR-MS in 2009 both measured a total monoterpene mixing ratio.

Several constraints in both 2008 and 2009 were set equal to the median mixing ratios reported for the PROPHET 1998 campaign (Table 5 in Tan et al., 2001). These include methane (CH4, 1.71 ppmv), ethane (ETH, 1 ppbv), ethylene (ETE, 0.18 ppbv), terminal and internal olefins (OLT, 0.42 ppbv and OLI, 0.17 ppbv), hydrogen peroxide (H_2O_2, 2 ppbv), and xylenes (XYL, 0.15 ppbv). Additional compounds in 2008 that were set equal to the 1998 data but were measured in 2009 are carbon monoxide (CO, 260 ppbv), less reactive aromatics consisting primarily of benzene and toluene (TOL, 0.29 ppbv), and ketones (KET, 4 ppbv). Median values of XYL, TOL, and KET were not reported in Table 5 of Tan et al. (2001), but were calculated directly from the 1998 dataset. For CABINEX 2009, small and less reactive hydrocarbons including saturated and substituted compounds (HC3) were set equal to the sum of the measured methanol mixing ratios and the 1998 mixing ratios of acetylene and C3+C4 alkanes. For PROPHET 2008, HC3 was set equal to 4.0 ppbv, which is the median of the 2009 measurements described above. Methanol mixing ratios (5-10 times higher than the other small HCs) dominated HC3 from this derivation. In both 2008 and 2009, more reactive hydrocarbons (HC5 and HC8) were set equal to 0.045 ppbv and 0.06 ppbv as estimated from the 1998 dataset.

Sec. S4 - Modeling Sensitivity Analysis

Table S3 shows results from a sensitivity analysis performed on the PROPHET 2008 and CABINEX 2009 models whereby all of the measured and estimated model constraints were independently increased or decreased by their 2σ uncertainty value and their effect on model OH and HO2 + ISOP concentrations observed. The 2σ uncertainty values for PROPHET 2008 and CABINEX 2009 are different (Table 2, main text) and unmeasured constraints were given a maximum 2σ uncertainty value of 95% to avoid setting a constraint at a zero value. All of the photolysis rates from 2008 were given a 2σ uncertainty value of 95% while the photolysis rates measured during CABINEX had 2σ uncertainty values of 60%. Aside from the photolysis rates, the modeled OH and HO2 + ISOP concentrations were found to be most sensitive to isoprene and to a lesser extent NO mixing ratios during the day. As a result, the analysis in this study only focuses on times of overlapping isoprene, NO, and HO_x measurements. A sensitivity analysis of the nighttime CABINEX model shows that in addition to isoprene, the modeled nighttime OH and HO2 + ISOP concentrations are sensitive to the mixing ratio of monoterpenes and internal olefins within their associated uncertainties.

Sec. S5 - Peroxy Radical Composition

Throughout this study, the measured HO_2* values are compared to the modeled HO2+ ISOP concentrations because isoprene peroxy radicals are the dominant hydroxy alkyl peroxy radical at the PROPHET site, and the conversion efficiency for isoprene peroxy radicals and several other hydroxy alkyl peroxy radicals has been measured in the lab to be approximately 90 ± 4%. However, at night isoprene peroxy radicals may not be the dominant hydroxy alkyl peroxy

radical, and as a result the measured HO_2* may reflect the influence of additional peroxy radical interferences. Figure S5 shows different model HO_2* compositions if additional RO_2 interferences were considered. The HO2 + αRO2 (full) trace (green) uses estimated conversion efficiencies based on the relative relationships of the conversion efficiency from Fuchs et al. (2011) and the ISOP conversion efficiency reported in this study:

HO2 + αRO2 (full) = HO2 + 90% x ISOP
+ 100% x (OLTP+OLIP+APIP+LIMP+XYLP+TOLP+ETEP) + 67% x MACP
+ 5% x (CH3O2+ACO3+KETP) + 8% x (ETHP+HC3P) + 31% x HC5P + 55% x HC8P

Preliminary laboratory measurements of the RO_2 interference from propane-RO_2 and trans-2-butene-RO_2 agree well with the relative relationship derivation for the RO_2 detection efficiencies. The HO2 + αRO2 (limited) trace (purple) is the same as the HO2 + αRO2 (full) trace but subtracts the peroxy radicals that derive from oxidation of highly reactive constrained, but unmeasured species, mostly of anthropogenic origin.

HO_2 + αRO_2 (limited) = HO2 + αRO_2 (full) – (OLTP+OLIP+XYLP)

Neither trace incorporates the NO_3-alkene adduct RO_2 surrogate species from RACM, OLNN + OLND. These NO_3-adducts are produced from oxidation by NO_3 of these same reactive anthropogenic alkenes and accumulate in mixing ratio at night in the low NO conditions of this study. Due to their accumulation and the uncertainty of their precursor concentration, the NO_3-adduct peroxy radicals were excluded from Figure S5.

Figure S5 shows that during the CABINEX daytime campaign median model, even the model HO2 + αRO2 (full) trace is within twice the relative standard deviations of the modeled HO2 + ISOP. When the more uncertain OLTP, OLIP, and XYLP species are removed, the HO2 + αRO2 (limited) trace agrees well with the model HO2 + ISOP. At night, the modeled HO2 + ISOP concentrations are approximately 30% higher than the measured HO_2* concentrations, well within the 2σ uncertainty of nighttime model concentrations. However, both of the expanded model HO_2* traces are outside of the 2σ relative uncertainty of the model HO2 + ISOP, with the HO2 + αRO2 (full) overpredicting the measured HO_2* by a factor of four. As mentioned in the main text, the RACM mechanism does not include a complete set of radical + radical termination reactions that may lead to an underprediction of the total termination rate of peroxy radicals at night. In addition, the underprediction of the measured HO_2* concentrations by the daytime CABINEX model may suggest that the model may be missing an important peroxy radical loss mechanism(s) that could also be important at night.

Sec. S6 – Nitrous Acid Imbalance vs. jHONO

Figure S6 displays the correlation between the above canopy HONO photolysis value at CABINEX and the HONO sink-source imbalance (jHONO x [HONO] – $k_{(OH+NO)}$ x [OH] x [NO]). The positive correlation between the HONO imbalance and the j-value supports the finding (Zhou et al. 2011) that an important photolytic source of HONO is not accounted for in this environment. Additional analysis of this correlation can be found in the Sec. 3.4 of the main text.

Sec. S7 – Observed to Model OH ratio vs. Isoprene and Nitric Oxide

Several previous studies have shown a dependence of the observed/model OH ratios on the mix-

ing ratio of isoprene (Ren et al., 2008; Kubistin et al., 2010) and NO (Tan et al., 2001; Lu et al., 2012). Figure S7 shows the daily 2 hour median observed-to-modeled OH ratios for CABINEX 2009 plotted versus the measured mixing ratios of NO and isoprene. As illustrated in this Figure, there does not appear to be a significant dependence of these ratios on the mixing ratio of isoprene or NO. The large variability in the observed-to-modeled OH ratio data for low mixing ratios of NO (< 20 pptv) and isoprene reflect the uncertainty associated with the values of OH near the limit of detection of the instrument, however a regression analysis does not reveal a significant trend in either of these plots (Figure S7). These results are in contrast to the analysis by Lu et al. (2012), where the observed-to-modeled OH ratios of five different OH instruments during different campaigns generally increased as isoprene mixing ratios increased above 400 pptv. Lu et al. (2012) also observed an increase in the observed-to-modeled OH ratio at NO mixing ratios of approximately 0.5 ppbv and below. Although all of the data in the present analysis are below 0.5 ppbv of NO, Figure S7 suggests that the observed to modeled ratio of OH is independent of NO for NO mixing ratios as low as 50-100 pptv.

References

Cantrell, C. A., Zimmer, A., and Tyndall, G. S.: Absorption cross sections for water vapor from 183 to 193 nm, Geophysical Research Letters, 24, 2195-2198, 10.1029/97gl02100, 1997.

Creasey, D. J., Halford-Maw, P. A., Heard, D. E., Pilling, M. J., and Whitaker, B. J.: Implementation and initial deployment of a field instrument for measurement of OH and HO2 in the troposphere by laser-induced fluorescence, J. Chem. Soc. Faraday T., 93, 2907-2913, 1997.

Creasey, D. J., Heard, D. E., and Lee, J. D.: Absorption cross-section measurements of water vapour and oxygen at 185 nm. Implications for the calibration of field instruments to measure OH, HO2 and RO2 radicals, Geophysical Research Letters, 27, 1651-1654, 10.1029/1999gl011014, 2000.

Creasey, D. J., Heard, D. E., and Lee, J. D.: OH and HO2 measurements in a forested region of north-western Greece, Atmospheric Environment, 35, 4713-4724, 10.1016/s1352-2310(01)00090-5, 2001.

Dusanter, S., Vimal, D., and Stevens, P. S.: Technical note: Measuring tropospheric OH and HO2 by laser-induced fluorescence at low pressure. A comparison of calibration techniques, Atmospheric Chemistry and Physics, 8, 321-340, 2008.

Faloona, I., Tan, D., Brune, W., Hurst, J., Barket, D., Couch, T. L., Shepson, P., Apel, E., Riemer, D., Thornberry, T., Carroll, M. A., Sillman, S., Keeler, G. J., Sagady, J., Hooper, D., and Paterson, K.: Nighttime observations of anomalously high levels of hydroxyl radicals above a deciduous forest canopy, Journal of Geophysical Research-Atmospheres, 106, 24315-24333, 10.1029/2000jd900691, 2001.

Faloona, I. C., Tan, D., Lesher, R. L., Hazen, N. L., Frame, C. L., Simpas, J. B., Harder, H., Martinez, M., Di Carlo, P., Ren, X. R., and Brune, W. H.: A laser-induced fluorescence instrument for detecting tropospheric OH and HO2: Characteristics and calibration, Journal of Atmospheric Chemistry, 47, 139-167, 10.1023/B:JOCH.0000021036.53185.0e, 2004.

Fuchs, H., Bohn, B., Hofzumahaus, A., Holland, F., Lu, K. D., Nehr, S., Rohrer, F., and Wahner, A.: Detection of HO2 by laser-induced fluorescence: calibration and interferences from RO2 radicals, Atmospheric Measurement Techniques, 4, 1209-1225, 10.5194/amt-4-1209-2011, 2011.

Hofzumahaus, A., Brauers, T., Aschmutat, U., Brandenburger, U., Dorn, H.-P., Hausmann, M., Heßling, M., Holland, F., Plass-Dülmer, C., Sedlacek, M., Weber, M., and Ehhalt, D. H.: Reply, Geophys. Res. Lett., 24, 3039-3040, 1997.

Holland, F., Aschmutat, U., Heßling, M., Hofzumahaus, A., and Ehhalt, D. H.: Highly time resolved measurements of OH during POPCORN using laser-induced fluorescence spectroscopy, J. Atmos. Chem., 31, 205-225, 1998.

Matsumi, Y., Kono, M., Ichikawa, T., Takahashi, K., and Kondo, Y.: Laser-Induced Fluorescence instrument for the detection of tropospheric OH radicals, B. Chem. Soc. Jpn., 75, 711-717, 2002.

Sander, S. P., Friedl, R. R., Barker, J. R., Golden, D. M., Kurylo, M. J., Wine, P. H., Abbatt, J. P. D., Burkholder, J. B., Kolb, C. E., Moortgat, G. K., Huie, R. E., Orkin, V. L.: Chemical Kinetics and Photochemical Data for Use in Atmospheric Studies, Evaluation Number 17, JPL Publication 10-6, NASA Jet Propulsion Laboratory, Pasadena, California, 2011.

Smith, S. C., Lee, J. D., Bloss, W. J., Johnson, G. P., Ingham, T., and Heard, D. E.: Concentrations of OH and HO2 radicals during NAMBLEX: measurements and steady state analysis, Atmospheric Chemistry and Physics, 6, 1435-1453, 2006.

Stevens, P. S., Mather, J. H., and Brune, W. H.: MEASUREMENT OF TROPOSPHERIC OH AND HO2 BY LASER-INDUCED FLUORESCENCE AT LOW-PRESSURE, Journal of Geophysical Research-Atmospheres, 99, 3543-3557, 10.1029/93jd03342, 1994.

Tan, D., Faloona, I., Simpas, J. B., Brune, W., Shepson, P. B., Couch, T. L., Sumner, A. L., Carroll, M. A., Thornberry, T., Apel, E., Riemer, D., and Stockwell, W.: HOx budgets in a deciduous forest: Results from the PROPHET summer 1998 campaign, Journal of Geophysical Research-Atmospheres, 106, 24407-24427, 10.1029/2001jd900016, 2001.

Tanner, D. J. and Eisele, F. L.: Present OH measurement limits and associated uncertainties, J. Geophys. Res., 100, 2883-2892, 1995.

Table S1: The suite of compounds used to constrain the modeled OH and HO_2 concentrations that were either measured or estimated from past measurements.

RACM Surrogate	PROPHET 2008	CABINEX 2009
H2O	measured	measured
Ozone (O3)	measured	measured
Nitrous Acid (HONO)	measured	measured
Nitric Oxide (NO)	measured	measured
Nitrogen Dioxide (NO2)	measured	measured
Isoprene (ISO)	measured	measured
Methacrolein+MVK (MACR)	measured	measured
Glyoxal (GLY)	measured	measured
Monoterpenes (API & LIM)	measured (median campaign values)	measured
Formaldehyde (HCHO)	measured & calculated (O3)	measured
Aldehydes (ALD)	calculated (HCHO)	measured
Methane (CH4)	Estimated (PROPHET 98)	Estimated (PROPHET 98)
Carbon monoxide (CO)	Estimated (PROPHET 98)	measured
Ketones (KET)	Estimated (PROPHET 98)	measured
Ethane (ETH)	Estimated (PROPHET 98)	Estimated (PROPHET 98)
Ethene (ETE)	Estimated (PROPHET 98)	Estimated (PROPHET 98)
Less reactive saturated HCs (HC3, HC5, HC8)	Estimated (PROPHET 98, CABINEX 09)	Measured (CABINEX 09) and Estimated (PROPHET 98)
Highly reactive unsaturated HCs (OLT & OLI)	Estimated (PROPHET 98)	Estimated (PROPHET 98)
Methyl Peroxide (OP1)	N/A	measured
Aromatic HCs (TOL & XYL)	Estimated (PROPHET 98)	Measured & estimated
Hydrogen Peroxide (H2O2)	Estimated (PROPHET 98)	Estimated (PROPHET 98)

Table S2: Data map showing availability of model constraints during the PROPHET 2008 and CABINEX 2009 campaigns. Each entry in the table represents a 6a-12p or 12p-9p time period for PROPHET 2008 or a 12a-12p or a 12p-12a time period for CABINEX. Green represents that more than 50% of the 15min time intervals in that period are supported by measurements, yellow = less than 50% supported by measurements, red = no modeling points supported by measurements. This study only used time periods where both NO and the isoprene measurements were available.

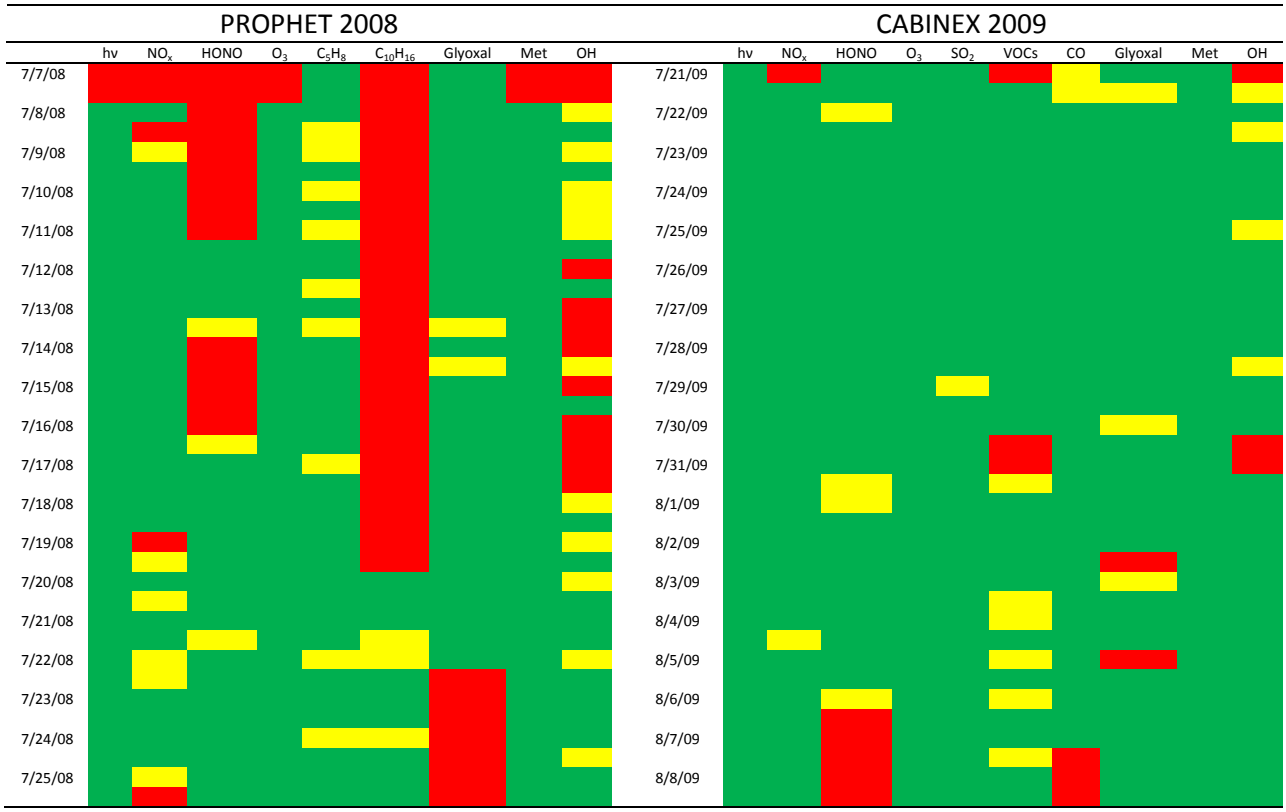

Table S3: PROPHET 2008 and CABINEX model sensitivity analysis showing key constrained components that the model OH and HO2+ISOP concentrations are most sensitive. Changes in OH and HO2+ISOP are given as relative changes from the base model. PROPHET 2008 values are the first entries in each cell and CABINEX values are the second.

RACM-MIM	**MORNING (10am)**		**AFTERNOON (3pm)**		**NIGHT (2am)**	
Constraint Concentrations	**OH (% change)**	**HO2+ISOP (% change)**	**OH (% change)**	**HO2+ISOP (% change)**	**OH (% change)**	**HO2+ISOP (% change)**
Carbon Monoxide (CO)	9, 2	3, <0.1	17, 4	3, <0.1	--, 5	--, 3
Alpha-pinene (API)	1, 1	<0.1, 2	2, <0.1	<0.1, <0.1	--, 13	--, 7
Nitric Oxide (NO)	5, 11	1, 2	15, 7	1, 1	--, 5	--, 1
Isoprene (ISO)	20, 14	7, 8	14, 10	7, 6	--, 6	--, 12
Internal Olefins (OLI)	4, 10	2, 14	11, 5	7, 6	--, 28	--, 18
Formaldehyde (HCHO)	<0.1, <0.1	5, 1	2, <0.1	11, 1	--, 1	--, <0.1
Aldehydes (ALD)	4, 1	2, 1	7, 2	3, 1	--, 1	--, <0.1
Hydrogen Peroxide (H2O2)	6, 4	3, 4	5, 2	3, 3	--, 1	--, 1
Photolysis Rates						
J(O3)→→OH+OH	51, 8	24, 8	20, 17	10, 11	--, --	--, --
J(HONO)→OH+NO	23, 8	11, 5	19, 6	8, 5	--, --	--, --
J(H2O2)→OH+OH	6, 3	3, 2	6, 2	3, 2	--, --	--, --
J(HCHO)→H+HCO	5, 1	6, 1	6, 1	11, 1	--, --	--, --

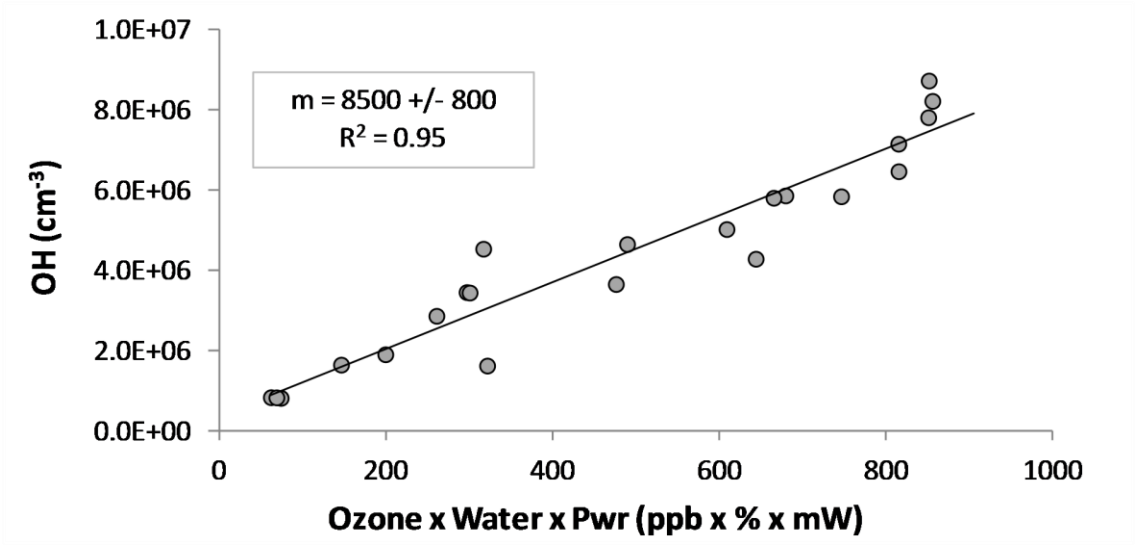

Figure S1: Photolytic Ozone x Water Interference dependance of the IU-FAGE instrument to measure OH. The 2σ uncertainty on the slope is (+/-) 800.

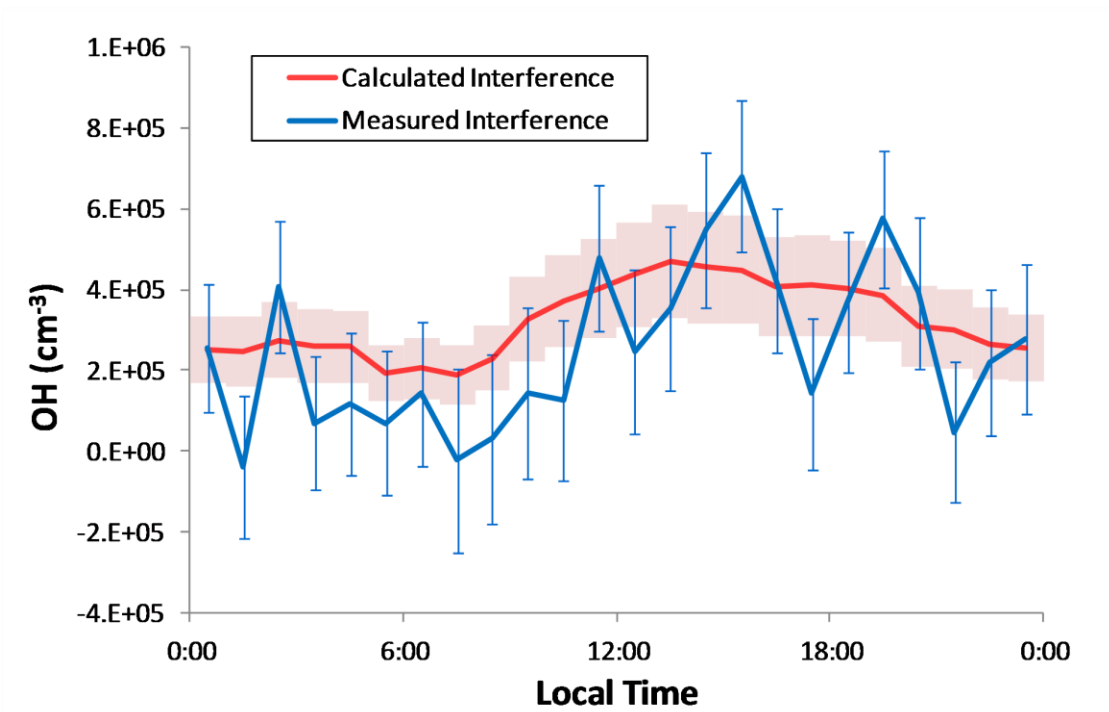

Figure S2: Median campaign data for ground-based measurements from the PROPHET site in 2010 compared to the calculated interference based on measured ozone, water, and laser power. The pink error bars represent 2σ uncertainty on the calculated interference and are based on the precision of the ozone, water, and power measurements along with the uncertainty from the slope in Figure S2. Blue error bars are 2σ uncertainty based on precision of the measurements

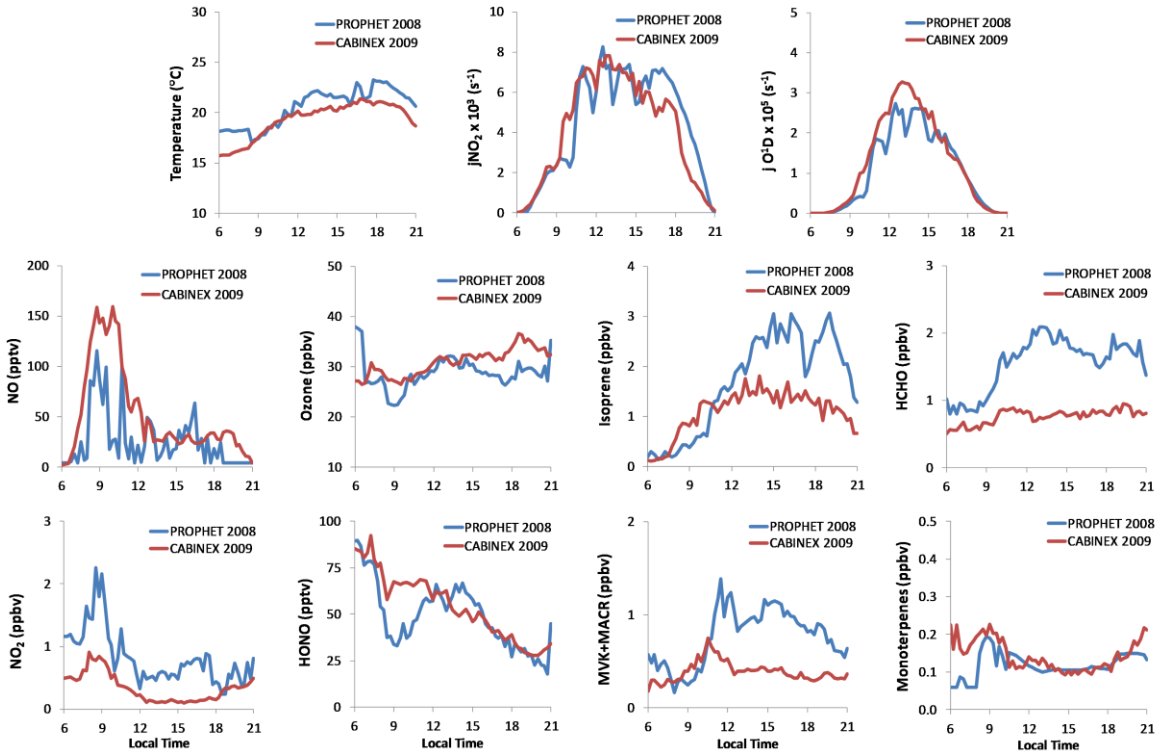

Figure S3: Median values of the primary model constraints for the PROPHET site during 2008 and CABINEX 2009 based on availability and overlap of key constraints (isoprene and NO) with OH.

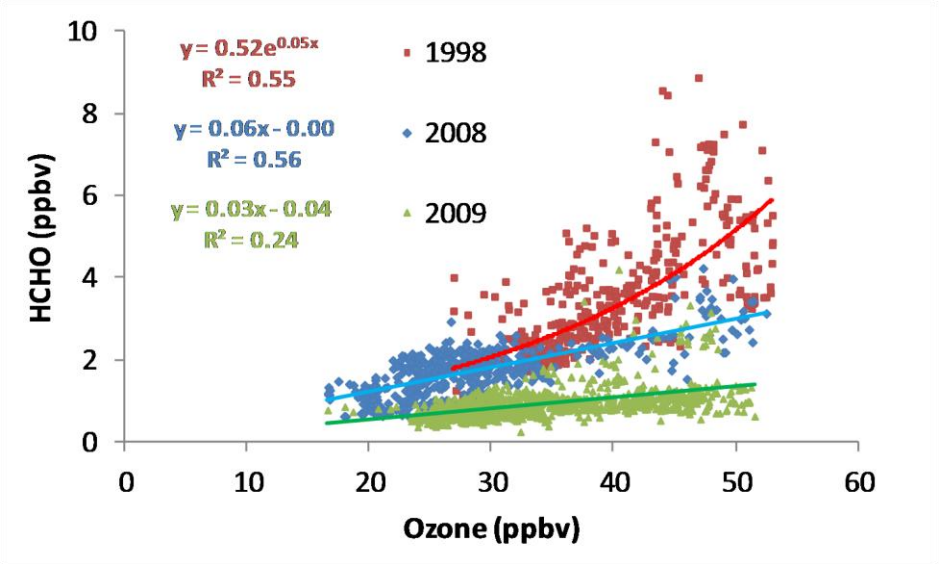

Figure S4: Correlation plot between ozone (< 53 ppbv) and formaldehyde to describe how day-time HCHO mixing ratios were estimated. Points in red are from the PROPHET 1998 dataset, blue points are from PROPHET 2008, and green points are from the CABINEX 2009 campaign.

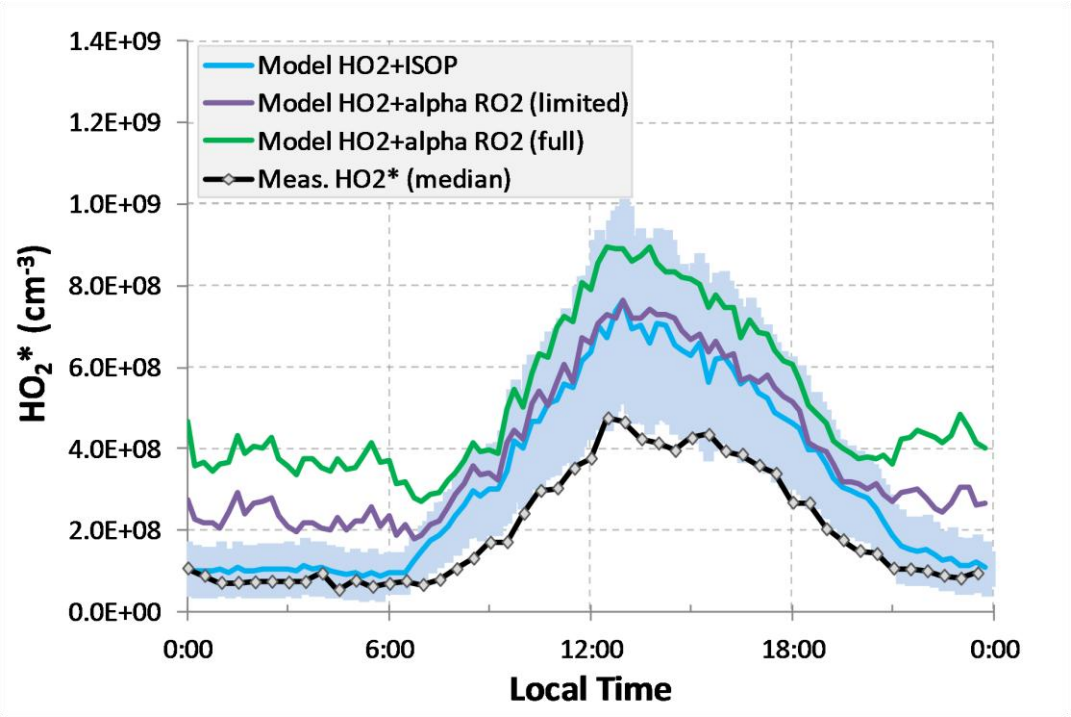

Figure S5: CABINEX median campaign measured HO_2* (black line w/ gray diamonds), model HO2+ISOP (blue), model HO2+αRO2 limited (purple), and model HO2 + αRO2 full (green). Light blue shaded region is the model HO2 + ISOP 2σ uncertainty (± 30% and ± 40% for day and night).

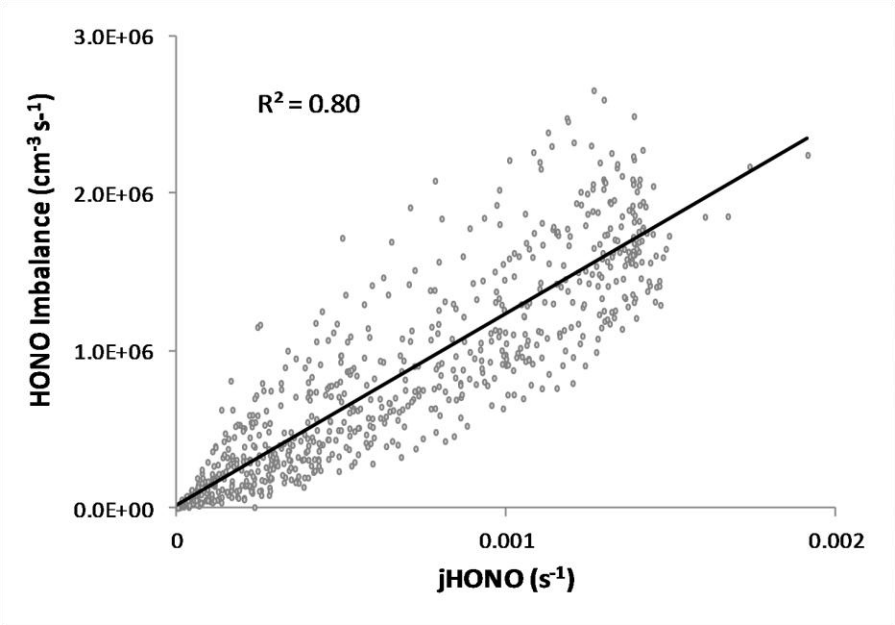

Figure S6: Correlation of the calculated CABINEX HONO imbalance and the measured HONO j-value above canopy.

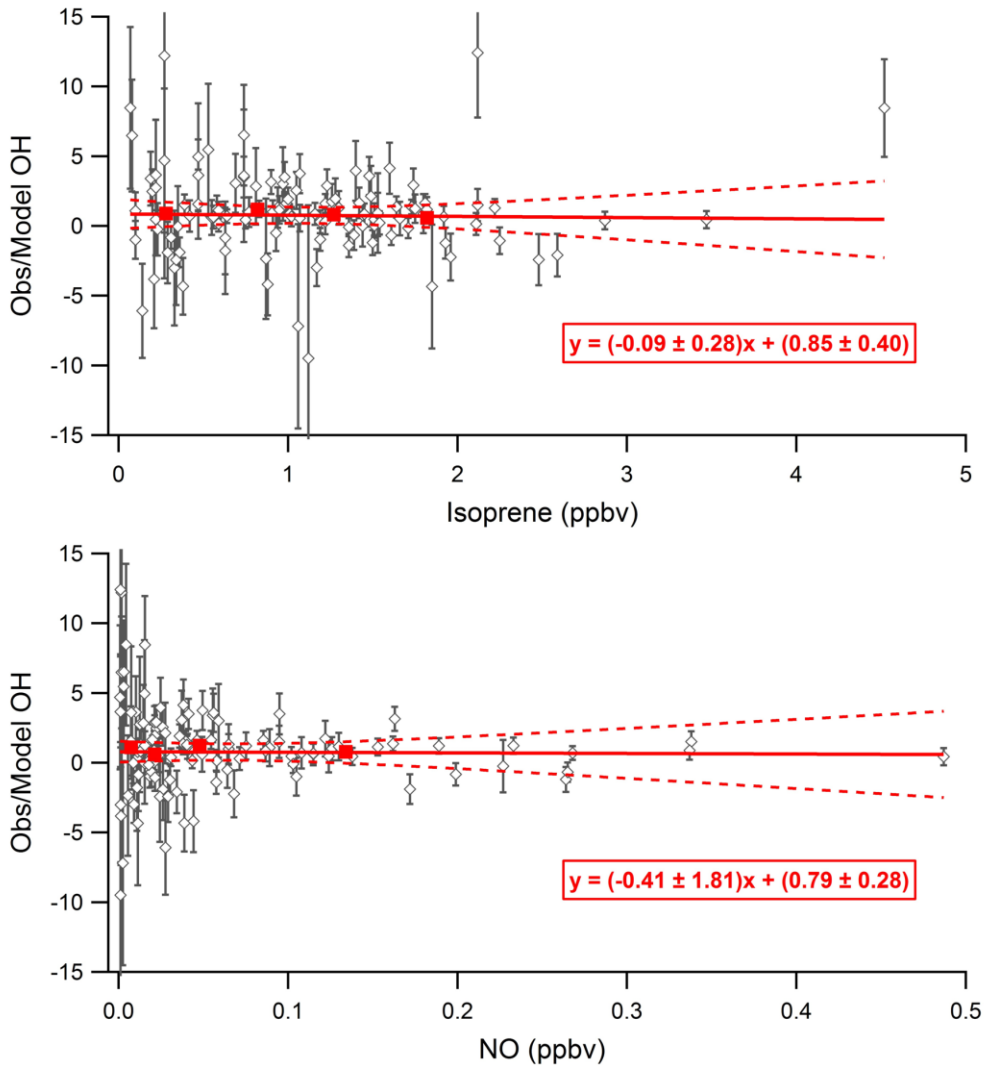

Figure S7: CABINEX observed (2 hour median) to model ratios of OH vs. NO and isoprene. Error bars reflect the propagation of the uncertainty on the measured and modeled OH values. The solid red line is a weighted regression of the data based on the uncertainty and the dashed red lines are the 95% confidence limits of the regression. The red squares are median ratios within 30 point bins of NO and isoprene.